



Experimental study on surface integrity of Inconel 690 milled by coated carbide inserts

Zhen Chen¹ · Chuanzhen Huang^{2,1} · Binghao Li¹ · Guoyan Jiang³ · Zhengyi Tang¹ · Jiahui Niu¹ · Hanlian Liu¹

Received: 8 March 2022 / Accepted: 30 May 2022 / Published online: 8 June 2022
© The Author(s), under exclusive licence to Springer-Verlag London Ltd., part of Springer Nature 2022

Abstract

One of the major concerns in the field of machinery manufacturing of Ni-based superalloys is machining-induced surface integrity, since the surface integrity is closely bound up with the service performance of machined components. In the current study, a range of orthogonal experiments are carried out to investigate the surface integrity characteristics, including surface morphology, surface roughness, residual stress, work hardening, and surface microstructure during high-speed milling of Inconel 690. The results show that both cutting speed and feed rate plays a constructive role in determining cutting force and surface integrity of Inconel 690. The cutting force displays a downtrend with the increase of cutting speed while presents an uptrend with the increase of feed rate as well as depth of cut. While, no clear tendency between the relative position of tool and workpiece and the cutting force could be found. The surface roughness decreases firstly and then increases slightly with the increase of cutting speed while increases with the increase of feed rate. The surface residual stress presents more tensile tendency as the cutting speed and feed rate increase. Similarly, the increased cutting speed and feed rate strengthen the degree of work hardening as well as depth of work hardening. It is worth mentioning that not only the depth of cut but also the relative position of tool and workpiece has little effect on surface integrity. Severe plastic deformation occurs in the microstructure of machined surface layer. No phase transformation is observed at all workpiece surface. This study provides a meaningful chance to achieve excellent machining-induced surface integrity via selecting suitable cutting parameters.

Keywords Inconel 690 · Surface integrity · Microstructural alteration · High-speed face milling · Cutting parameters

1 Introduction

It is well known that nickel-based superalloy has a high melting point, high ductility, excellent high-temperature mechanical and chemical properties, outstanding resistance to fatigue and corrosion, and good thermal stability. Owing to these attractive properties, it can perform well

under hostile working conditions, which becomes the competitive candidate material for a wide range of industries such as aerospace, shipbuilding, nuclear power plants, and petrochemical industry [1]. However, the machinability of nickel-based superalloy is very poor, only 10–20% of AISI 1045 steel due to the low heat capacity and thermal conductivity, high hot hardness, high-temperature strength, and the presence of abrasive particles in the material microstructure. These limitations make it pose a series of considerable challenges during machining, such as high cutting temperature and cutting force, intense plastic deformation, severe work hardening, the premature emergence of tool wear, and the difficulty to control dimensional accuracy [2].

Machined-induced surface integrity is generally considered as the combinations of mechanical, chemical, morphological, and metallurgical characteristics of a component surface obtained from specific machining process [3, 4]. Components are generally subjected to high thermal loads, high mechanical loads, and corrosion during the intended applications. Through analyzing the service

✉ Chuanzhen Huang
huangchuanzhen@ysu.edu.cn

¹ Center for Advanced Jet Engineering Technologies (CaJET), Key Laboratory of High-Efficiency and Clean Mechanical Manufacture (Ministry of Education), National Experimental Teaching Demonstration Center for Mechanical Engineering (Shandong University), School of Mechanical Engineering, Shandong University, Jinan 250061, China

² School of Mechanical Engineering, Yanshan University, Qinhuangdao 066004, China

³ Dongfang Electric (Guangzhou) Heavy Machinery Co, Ltd, Guangzhou 511455, China

history of dynamic components, it can be found that severe failures caused by fatigue, stress corrosion cracking, wear and creep almost originate from the surface or subsurface of components [5]. Therefore, the surface integrity of components is of vital importance for the service performance in practical applications. How to ameliorate the surface integrity of machined components, extend the service life of critical parts, and improve the reliability of dynamic components have always been a research hotspot in mechanical engineering.

Surface morphology is comprised of surface roughness, surface waviness, and surface defects. Several published studies indicated that surface defects mainly included surface cavities [6, 7], grooves [6], feed marks [8, 9], smearing [10], tearing [11], side flow [7], and metal debris [9] during machining of nickel-based super alloys. The existence of these types of surface defects will harm the subsequent service performance of machined components. Surface roughness refers to the surface high-frequency irregularities, which is considered as the most widely used evaluation parameters of surface integrity [12]. In this context, Umbrello [13] explored the influence of cutting conditions on the surface integrity in dry turning of Inconel 718 and found that surface roughness gradually reduced with the rise of cutting speed, while increased with the increment of feed rate. Nevertheless, Thakur et al. [9] figured out a converse result claiming that the surface roughness displayed an upward trend when the cutting speed increased during dry turning of Ni-based superalloy Incoloy 825. The main reason for this divergence was the occurrence of tool wear during the cutting process. Li et al. [14] studied the surface integrity under both dry condition and minimum quantity lubricant (MQL) condition in milling of Inconel 718 and pointed out that there was no apparent correlation between depth of cut and surface roughness. Diniz et al. [15] found that the effect of the relative position of tool and workpiece on the surface roughness was not strong in face milling of AISI 1045 steel.

Concerning surface metallurgy, it refers to the microstructural alterations occurred in the machined surface layer, including white layer formation, plastic deformation, and grain refinement and so on [3]. In order to investigate the metallurgical characterization of the machined surface and subsurface, Imran et al. [16] performed the micro-drilling experiments of nickel-base superalloy Inconel 718. These results indicated that increase in cutting speed and feed rate resulted in a slight rise in the white layer thickness. Jiang et al. [17] studied the microstructural characteristics of turning high-strength alloy steel under different cutting speeds. They found that the cutting speed had a significant effect on the graded deformational microstructure of machined surface layer, and the higher speed

condition could enhance dislocation strengthening and fine grain strengthening.

The mechanical characteristics of machining-induced surface integrity mainly refer to the changes of mechanical properties which are typically manifested as the residual stress and hardness. The influences of milling parameters on the surface residual stress during high-speed machining of Inconel 718 were studied by Cai et al. [18]. High tensile residual stress appeared at the machined surface. Also, higher cutting speed tended to result in higher tensile residual stress. These results are consistent with those found by Ezilarasan et al. [8] when turning Nimonic C-263 with whisker-reinforced ceramic cutting tools. Hua et al. [19] examined the residual stress at the machined surface during face turning of Inconel 718, and pointed out the residual stress at the machined surface tended to become more tensile with the feed rate getting larger. According to the research results of Hua and Liu [20], the degree of work hardening (DWH) of the machined surface was strengthened with an increase in cutting speed and feed rate. Moreover, the depth of work hardening indicated an increasing trend with increasing feed rate. However, the depth of work hardening did not change with cutting speed variation. In the same context, a different result claiming that the depth of work hardening in machining of Inconel 718 tended to decline with an increase in cutting speed was found by Pawade et al. [21]. Besides, they also suggested that the DWH enhanced significantly as the depth of cut increased, whereas the depth of work hardening decreased as the depth of cut increased.

According to the literature review above, it is in evidence that the wide and in-depth research work has been carried out on the surface integrity during machining of nickel-base superalloys, mainly focusing on Inconel 718. Inconel 690, a member of nickel-based superalloys and with a high Cr content, has been extensively employed in various engineering applications including nuclear reactors, turbines and combustion systems due to its good formability, excellent high-temperature mechanical properties, and superb corrosion resistance [22, 23]. Recently, a series of end-milling experiments of Inconel 690 were carried out by Sen et al. [24, 25] and Makhesana et al. [26] under MQL conditions. They focused on the influences of various lubricants on machining performances of Inconel 690, and assessed the cutting force, cutting temperature, tool life and surface roughness. However, few of the previously published studies have specifically investigated the surface integrity during high-speed machining of Inconel 690, despite its significance. Besides, there are hardly any studies regarding the effect of the relative position of tool and workpiece on surface integrity during the face milling operation.

In the present work, the comprehensive evaluation of different characteristics of surface integrity consisting of surface morphology, surface roughness, residual stress, work

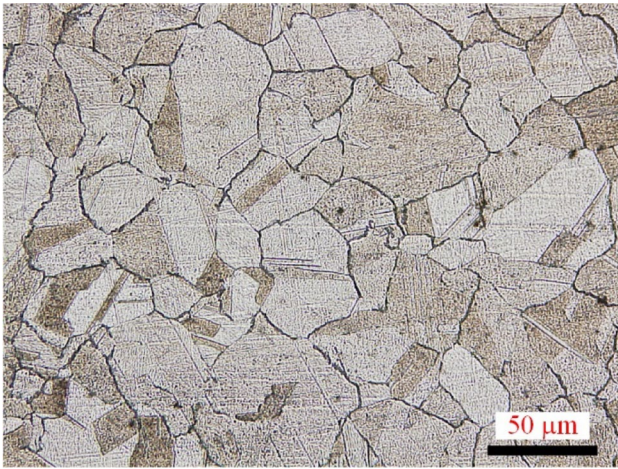


Fig. 1 Microstructure of Inconel 690

hardening, and surface microstructure during high-speed face milling of Inconel 690 was carried out. The effects of cutting speed, feed rate, depth of cut and relative position of tool and workpiece on the surface integrity were investigated in detail. The microstructural alteration in the machined surface layer generated by milling Inconel 690 was revealed.

2 Materials and experimental procedures

The workpiece material used in the current study is Ni-based superalloy, Inconel 690, with the dimensions of 102 mm × 65 mm × 100 mm, provided by Dongfang Electric Group (China). The material was solution annealed and water quenched, and its microstructure is presented in Fig. 1. The chemical composition of Inconel 690 is presented in Table 1, and the physical and mechanical properties are shown in Table 2.

As illustrated in Fig. 2, a CNC machining center DAEWOO ACE-V500 (South Korea) was introduced to conduct all the milling tests under dry conditions. The cutting tools used were AlTiCrN PVD-coated carbide inserts (ODHW0606AEN JC8015, DIJET, Japan) with high coating adhesion and good wear resistance, which were mounted onto the face milling cutter (OCT-06100-32R, DIJET, Japan) with the diameter of 100 mm. The mounted cutting tool has the rake angle $\gamma = 10^\circ$, the relief angle $\alpha = 5^\circ$, the nose radius $r = 1.2$ mm, and the cutting edge radius $r_e = 0.05\text{--}0.08$ mm. All the cutting experiments were carried out with new inserts to eliminate the effect of tool wear, and only single insert was fixed onto the milling cutter to avoid the clamped position error.

Table 2 Physical and mechanical properties of Inconel 690 at room temperature

Yield strength (MPa)	Tensile strength (MPa)	Elongation (%)	Reduction of area (%)	Thermal conductivity (W/m·k)	Hardness (HV0.3)
347	636	45	40	13.9	183.2 ± 4.8

In order to roundly study the influences of cutting speed, feed rate, depth of cut, and relative position of tool and workpiece on surface integrity in milling of Inconel 690, Taguchi L_9 (3^4) orthogonal arrays experiments were employed in this study. The interaction of each factor was neglected. The L_9 (3^4) orthogonal test layout was presented in Table 3. The levels of the cutting parameters were selected according to our pre-experiments and the recommendations from the insert manual as presented in Table 4. The minimum values of cutting speed and feed rate (level 1) were determined by comprehensively considering the recommended values of the tool manufacturers for machining nickel-based alloys and the values used in studies on machining of Inconel 690 [24–26]. The higher levels (level 2 and 3) were appropriately extended from the minimum values. In addition, the appropriate tool life was also taken into account when selecting the levels of cutting parameters. The pre-experiments on tool wear in dry machining of Inconel 690 were carried out at the maximum cutting parameters levels ($v_c = 270$ m/min, $f_z = 0.15$ mm/tooth, $a_p = 1$ mm) and minimum cutting parameters levels ($v_c = 90$ m/min, $f_z = 0.05$ mm/tooth, $a_p = 0.5$ mm). The single-tooth cutting and down-milling were adopted in both groups of pre-experiments. It was found that with the flank wear criterion of 0.3 mm, the tool life for the maximum and minimum cutting parameters levels exceeded 4 min and 30 min, respectively, thus justifying the chosen cutting parameters levels in terms of tool life. The depth of cut was selected at the levels of 0.5 mm, 0.75 mm, and 1 mm, corresponding to the semi-finishing condition. For each milling test, the width of cut a_c was maintained at 65 mm. The ratio of the cutter diameter and the width of cut was 1.54, within the range recommended by the DIJET tool manufacturer. As shown in Fig. 3, the relative position of tool and workpiece was defined as the distance between the end of the cutter diameter and the beginning of the workpiece, which was in accordance with the previous work [15]. It was worth noticing that tool failure occurred in a very short time under up-milling operation based on our pre-experiments. Therefore, the up-milling operation was not adopted in this study. The values of j parameter of 17.5 mm,

Table 1 Chemical composition of Inconel 690 (wt.%)

C	Si	Mn	P	S	Cr	Fe	Cu	Ti	Al	Ni
0.014	0.29	0.32	0.005	0.001	29.59	10.07	0.008	0.13	0.089	Balance

Fig. 2 Face milling experiments setup



26.25 mm, and 35 mm correspond to symmetric milling, partial asymmetric down-milling and completely asymmetric down-milling operations, respectively.

As depicted in Fig. 2, the Kistler 9257B three-component piezoelectric dynamometer (Switzerland) was employed to record the real-time cutting forces. For each test, the sampling time and sampling frequency were set to 20 s and 10,000 Hz, respectively.

During the face milling process, the cutting thickness changes continuously as the cutter rotates so that there are some discrepancies in surface integrity at different positions. Therefore, all surface integrity indicators, including surface morphology, surface roughness, residual stress, work hardening, and surface microstructure were measured at the vicinity of the locus of the cutter center in this study.

Table 3 L_9 (3^4) orthogonal design

Test	Factor A	Factor B	Factor C	Factor D
No.1	1	1	1	1
No.2	1	2	2	2
No.3	1	3	3	3
No.4	2	1	3	2
No.5	2	2	1	3
No.6	2	3	2	1
No.7	3	1	2	3
No.8	3	2	3	1
No.9	3	3	1	2

The machined surface morphology was obtained by a 3D laser confocal scanning microscope (VK-X200K, KEYENCE, Japan). With the assistance of the roughness-specific mode of the microscope, the machined surface roughness Sa was measured based on ISO 25178 by analyzing the obtained surface image. For each experiment, the average value of surface roughness was calculated by measuring five different specimen locations to assure reliability.

The measurements of machined surface residual stress along both the cutting speed direction σ_{xx} and the feed direction σ_{yy} were carried out on an X-ray diffraction (XRD) residual stress measurement device (iXRD COMBO, PROTO, Canada) on the basis of the $\sin^2\psi$ technique. The X-ray diffractometer used Cr-K β radiation from a source operated at 20 kV and 4.1 mA to acquire the (hkl = 311) diffraction peak at diffraction angle $2\theta = 149^\circ$. Three different micro-area of each machined surface were gauged to average the

Table 4 Cutting parameters and their levels

Factor	Cutting parameters	Level		
		1	2	3
A	Cutting speed v_c (m/min)	90	180	270
B	Feed rate f_z (mm/tooth)	0.05	0.1	0.15
C	Depth of cut a_p (mm)	0.5	0.75	1
D	Relative position of tool and workpiece j (mm)	17.5	26.25	35

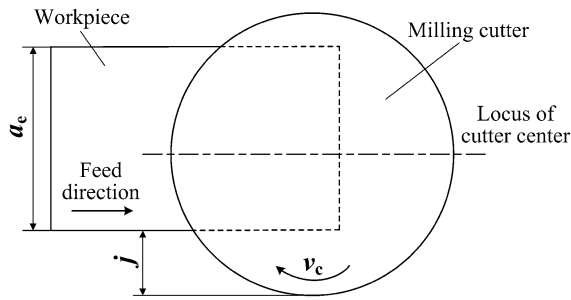


Fig. 3 Schematic about the relative position of tool and workpiece

residual stress results. The microhardness measurements of the machined surface were conducted on a Vickers microhardness tester (DHV-1000Z, China) with a load of 300 g for the duration of 15 s. The average value was obtained by repeated measurement for five times under each cutting configuration. In order to measure the nano-hardness in the depth direction of machined surface, the sections of the workpiece (8 mm × 5 mm × 5 mm) after machining were obtained by wire electrical discharge machining (WEDM) from the locus of cutter center as shown in Fig. 4. Then, the test specimens were mounted in bakelite powder, ground utilizing silicon carbide papers with grits size of 400–1500 mesh and polished using diamond micro powder with 0.25 μm. Subsequently, a nano-indenter (Hysitron TI980, Bruker, UK) was employed to determine in-depth nano-hardness at a load of 10 mN. The duration period at maximum load was 5 s. The starting position of nano hardness measurement was located at 3 μm below the machined surface. The distance between each indentation

and the next indentation was also maintained at 3 μm along the depth direction of the machined surface until reaching the nano-hardness value of block material. In addition, at the same depth, five indentations were made at an interval of 4 μm to guarantee the reliability of measured results.

The cross sections of machined surface for Inconel 690 after finely polishing were chemically etched using a solution made up of 10 g copper sulfate, 10 mL sulfuric acid, and 100 mL hydrochloric acid. The etching time was controlled in the range of 5–8 s. A scanning electron microscope (SEM, SUPRA™ 55, ZEISS, Germany) was employed to evaluate the microstructure alterations of machined workpiece in the superficial surface layer.

In order to characterize the crystalline structures of machined surface, an X-ray diffractometer (DMAX-2500PC, Japan) was employed. Since the diffraction peak intensity is affected by the measurement area, the XRD measurement was performed on an area as large as about 12 mm × 12 mm on the machined surface. The scanning angle was 30 ° to 100 °, and the scanning speed was 8 °/min.

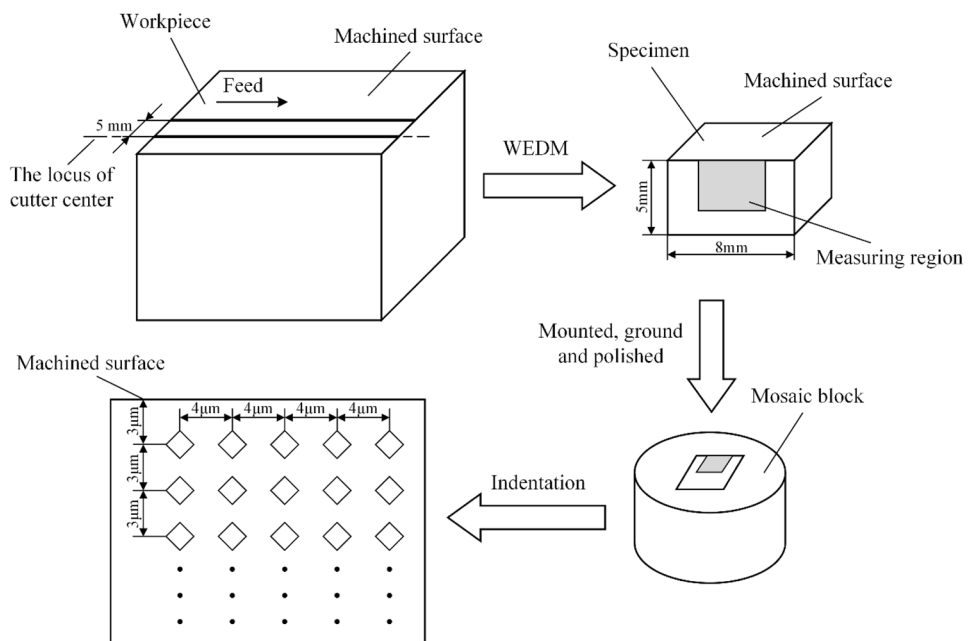
R_v , R_f , R_a , and R_j represent the sensitivity values of cutting speed, feed rate, depth of cut, and relative position of tool and workpiece for various experimental results respectively, which can be calculated with Eq. (1).

$$R_v = \max(K_{v1}, K_{v2}, K_{v3}) - \min(K_{v1}, K_{v2}, K_{v3})$$

$$R_f = \max(K_{f1}, K_{f2}, K_{f3}) - \min(K_{f1}, K_{f2}, K_{f3}) \tag{1}$$

$$R_a = \max(K_{a1}, K_{a2}, K_{a3}) - \min(K_{a1}, K_{a2}, K_{a3})$$

Fig. 4 The schematic diagram of in-depth nano-hardness measurements



$$R_j = \max(K_{j1}, K_{j2}, K_{j3}) - \min(K_{j1}, K_{j2}, K_{j3})$$

where K_{v1} , K_{v2} , and K_{v3} signify the mean values of the experimental results corresponding to the cutting speed at the level 1, 2, and 3, respectively. K_{f1} , K_{f2} , and K_{f3} represent the average values of the experimental results corresponding to the feed rate at the level 1, 2, and 3, respectively. K_{a1} , K_{a2} , and K_{a3} signify the experimental results' average values corresponding to the depth of cut at the level 1, 2, and 3, respectively. K_{j1} , K_{j2} , and K_{j3} represent the average values of the experimental results corresponding to the relative position of tool and workpiece at the level 1, 2, and 3, respectively. The above twelve parameters can be expressed with Eq. (2).

$$K_{v1} = \frac{Y_1 + Y_2 + Y_3}{3}$$

$$K_{v2} = \frac{Y_4 + Y_5 + Y_6}{3}$$

$$K_{v3} = \frac{Y_7 + Y_8 + Y_9}{3}$$

$$K_{f1} = \frac{Y_1 + Y_4 + Y_7}{3}$$

$$K_{f2} = \frac{Y_2 + Y_5 + Y_8}{3}$$

$$K_{f3} = \frac{Y_3 + Y_6 + Y_9}{3}$$

$$K_{a1} = \frac{Y_1 + Y_5 + Y_9}{3}$$

$$K_{a2} = \frac{Y_2 + Y_6 + Y_7}{3}$$

$$K_{a3} = \frac{Y_3 + Y_4 + Y_8}{3}$$

$$K_{j1} = \frac{Y_1 + Y_6 + Y_8}{3}$$

$$K_{j2} = \frac{Y_2 + Y_4 + Y_9}{3}$$

$$K_{j3} = \frac{Y_3 + Y_5 + Y_7}{3}$$

where Y_i is the measured value of various experimental results under each combination of cutting parameters separately, $i = 1, 2, 3, \dots, 7, 8, 9$.

3 Results and discussion

The results of the resultant cutting force F_R , surface roughness Sa , surface residual stress along the cutting speed direction σ_{xx} , surface residual stress along the feed direction σ_{yy} , and microhardness of the machined surface MH_s are illustrated in Table 5 under each combination of cutting parameters.

3.1 Cutting force

As one of the significant physical quantities in the cutting process, cutting force affects the chip formation process and the generation of cutting heat directly, and further affects tool wear, machining accuracy and machining-induced surface integrity. The influence trends of different cutting parameters on cutting force are shown in Fig. 5. The resultant cutting force was equal to the extraction of the square root of the square sum of the force components in three directions. As depicted in Fig. 5a, the cutting force shows a downward trend with the increment of cutting speed. As the

Table 5 Experimental results under various combinations of cutting parameters

Tests	Experimental results				
	F_R (N)	Sa (μm)	σ_{xx} (MPa)	σ_{yy} (MPa)	MH_s (HV0.3)
No.1	158.8 \pm 5.6	0.297 \pm 0.041	351 \pm 34	150 \pm 21	267.8 \pm 6.3
No.2	359.9 \pm 5.5	0.405 \pm 0.058	445 \pm 31	247 \pm 35	282.1 \pm 8.6
No.3	543.9 \pm 9.2	0.446 \pm 0.026	533 \pm 25	385 \pm 24	302.5 \pm 8.8
No.4	251.1 \pm 4.3	0.266 \pm 0.035	380 \pm 36	181 \pm 40	280.3 \pm 11.3
No.5	192.6 \pm 2.8	0.293 \pm 0.027	469 \pm 29	259 \pm 35	286.8 \pm 7.8
No.6	405.5 \pm 6.7	0.302 \pm 0.043	564 \pm 28	418 \pm 24	294.8 \pm 8.2
No.7	172.8 \pm 3.1	0.220 \pm 0.039	395 \pm 36	203 \pm 41	287.5 \pm 10.2
No.8	383.9 \pm 9.0	0.360 \pm 0.032	495 \pm 38	275 \pm 36	298.6 \pm 9.9
No.9	266.4 \pm 7.9	0.420 \pm 0.067	571 \pm 40	445 \pm 20	309.4 \pm 11.3

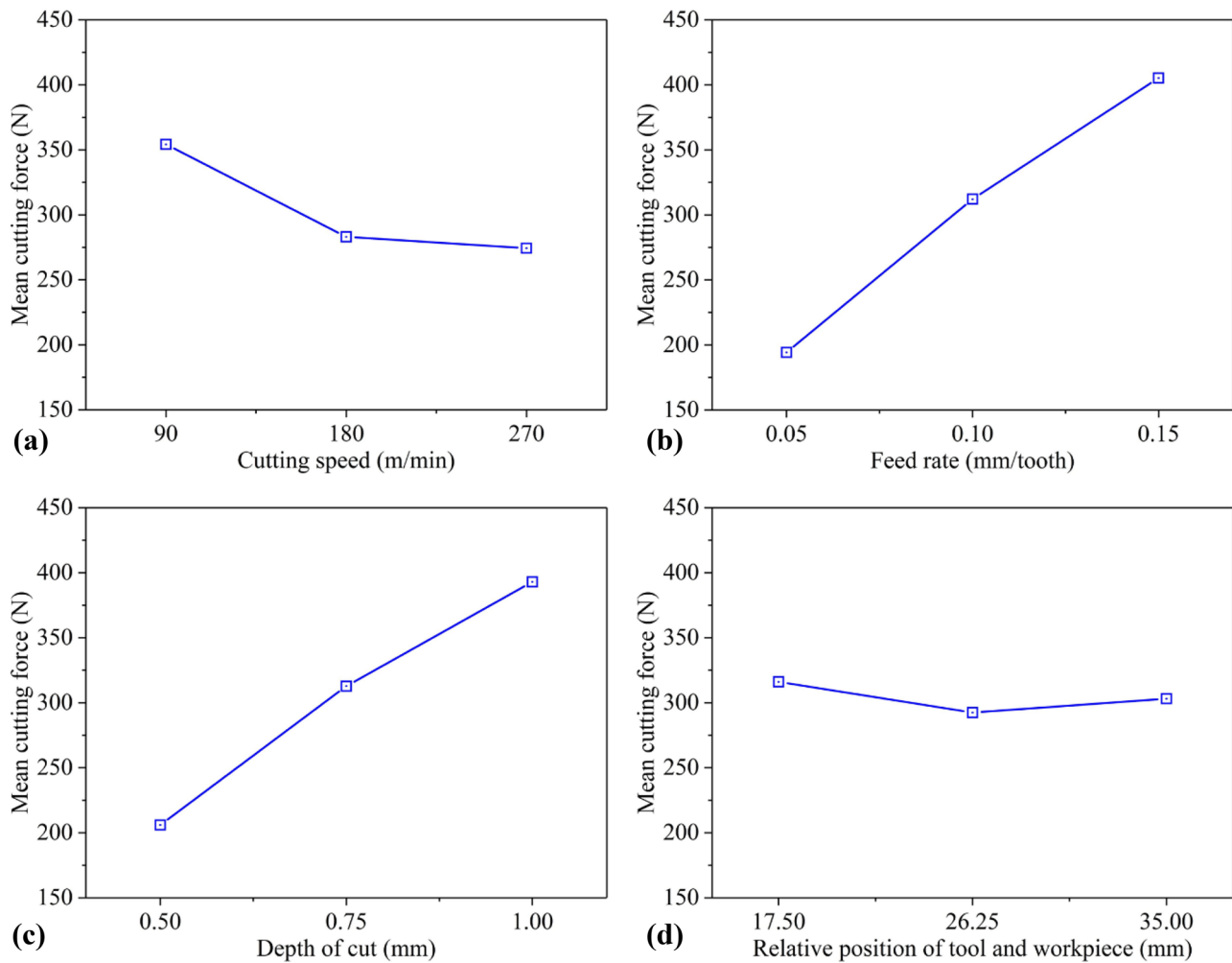


Fig. 5 Influence trends of different cutting parameters on cutting force. **a** Cutting speed. **b** Feed rate. **c** Depth of cut. **d** Relative position of tool and workpiece

cutting speed is raised at initial stage, the cutting force drops faster. However, when the cutting speed is raised further, the cutting force drops slightly. The reason is that with the increase of cutting speed at initial stage, the cutting temperature rises rapidly. This results in a strengthening of thermal softening effect to be much stronger than work hardening effect caused by the increase of the strain and strain rate in the primary shear zone [5]. Moreover, the friction angle of rake face decreases with elevation of cutting speed, resulting in the increasing shear angle. And the reduction of chip thickness with the increase of shear angle makes chip deformation coefficient decrease, leading to the reduction of cutting force. Accordingly, the cutting force decreases rapidly. However, when the cutting speed is still raised, the contact time between tool and workpiece becomes short. The cutting heat transferred into the workpiece material is reduced, causing the drop of the temperature in the cutting deformation

zone. Consequently, the gradual weakening of thermal softening effect makes the reduction of cutting force tend to be slow. As shown in Fig. 5b and c, both feed rate and depth of cut impact the cutting force in a significant way. The increment in feed rate and depth of cut produces the increment of material removal volume, leading to a higher cutting force. It can be seen from Fig. 5d that the relative position of tool and workpiece has little effect on cutting force. The reason may be that an interrupted cutting cycle, that is, one revolution of the tool, can be divided into cutting time and non-cutting time. The tool and workpiece are in the heat accumulation stage during the cutting time, and in the heat dissipation stage during the non-cutting time [27]. The ratio of the cutting time to the non-cutting time remains constant when the radial width of cut is fixed. In other words, the heat accumulation and dissipation between tool and workpiece are in a steady-state, resulting in a relatively stable

Table 6 Analysis and calculation of cutting force

Level	v_c (m/min)	f_z (mm/tooth)	a_p (mm)	j (mm)
1	354.2 (K_{v1})	194.3 (K_{f1})	205.9 (K_{a1})	316.1 (K_{j1})
2	283.1 (K_{v2})	312.1 (K_{f2})	312.8 (K_{a2})	292.5 (K_{j2})
3	274.4 (K_{v3})	405.3 (K_{f3})	393.0 (K_{a3})	303.1 (K_{j3})
R	79.8 (R_v)	211.0 (R_f)	187.0 (R_a)	23.6 (R_j)
Rank	3	1	2	4

cutting temperature during the cutting process. Therefore, cutting force is less affected by the relative position of tool and workpiece.

As presented in Table 6, the R value indicates the changing amplitude of the experimental result when the level of relevant factor changes, which reflects the influence degree of the factor on the target. The more considerable R value means that the corresponding cutting parameter has a greater impact on the test index. Hence, the effect order of different cutting parameters on the cutting

force is f_z , a_p , v_c , and j for the range of tested conditions. The best combination of cutting parameters corresponding to the minimum resultant cutting force is $v_{c3}f_{z1}a_{p1}j_2$ for the range of tested conditions.

3.2 Surface morphology

The machined surface morphology of Inconel 690 under different cutting conditions is displayed in Fig. 6. It is observed that the machined surface is characterized by regular peaks and valleys, which is because that the symmetrical surface morphology is generated by utilizing a single cutting edge with finite geometry during the cutting process [28]. The formation of peak-valley characteristics not only increases the specific surface area of the workpiece surface but also raises the risk of stress concentration on the workpiece surface, thus affecting the fatigue life and corrosion resistance of the workpiece surface. The typical surface defects in face milling Inconel 690 mainly involve feed marks, surface tearing, and ploughing grooves, indicating the machined surface

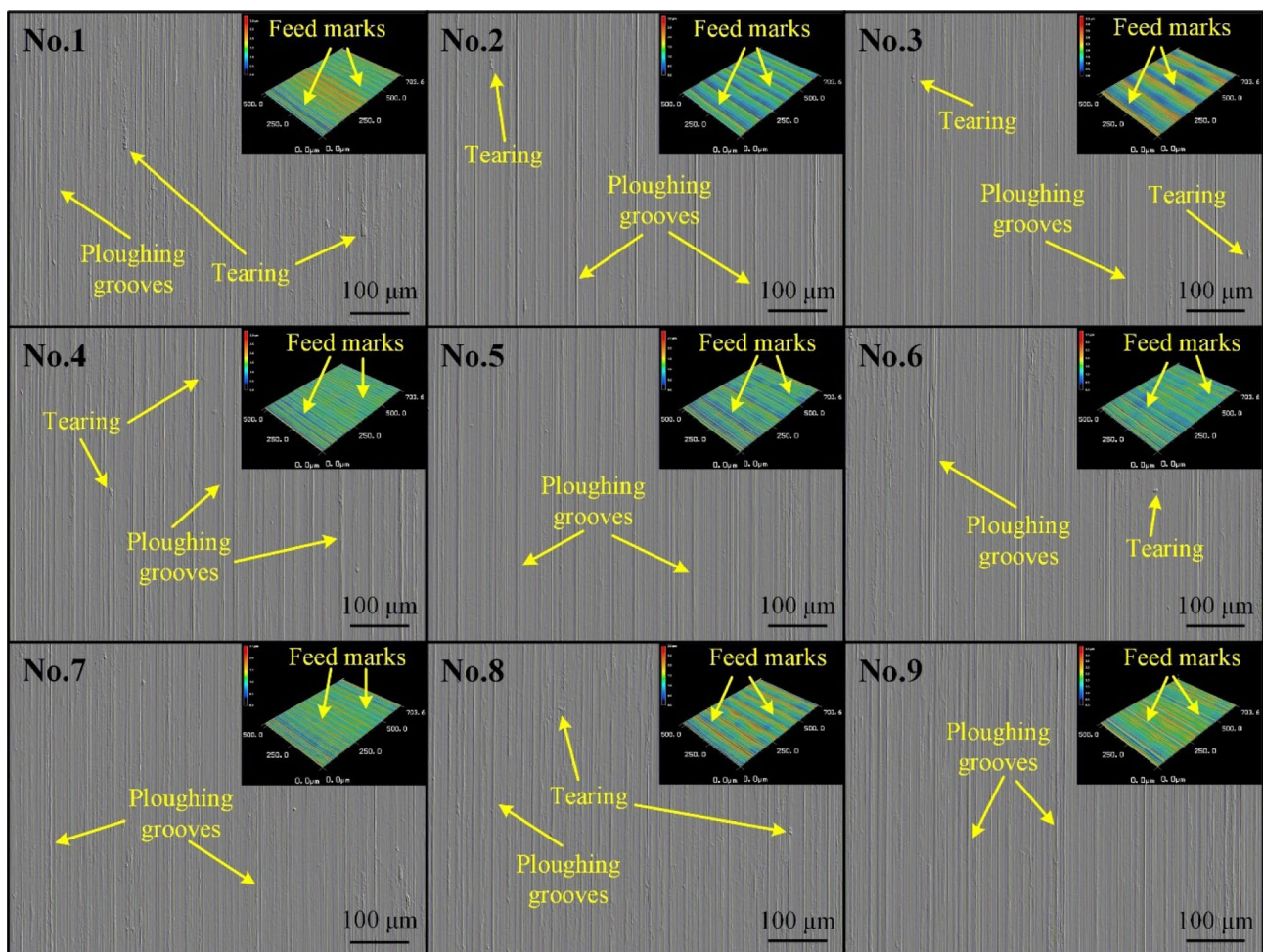


Fig. 6 The machined surface morphology under all cutting conditions

morphology is tightly associated with the material properties and the cutting parameters. Comparing the machined surface defects under all cutting configurations, it can be detected that the surface quality of test No.7 is the best, while the surface quality of test No.3 is the worst. This is further proved by the surface roughness values under various cutting conditions in Table 5.

3.3 Surface roughness

The measured values of surface roughness Sa under all cutting conditions are comparatively small as listed in Table 5. There are two main reasons for such a phenomenon. For one, a little end cutting edge angle of the tool insert makes the end cutting edge play the role of wiper in the workpiece surface generation, reducing the residual height of machined surface. For another, the machined surface roughness benefits from the chips flying off the machined surface.

The influence of cutting speed on surface roughness is graphically illustrated in Fig. 7a. It is discovered that surface roughness exhibits the trend of decreasing firstly and then increasing as the cutting speed is gradually increased, which is similar to the results found by Devillez et al. [5] who performed dry turning tests of Inconel 718 using coated carbide tools. As the cutting speed increases in the lower speed range, the dropping tendency of surface roughness can be ascribed to the decrease of built-up edge (BUE) and cutting force induced by the thermal softening phenomenon. The increasing effect of cutting speed in the higher speed range may be attributed to the occurrence of tool wear. From Fig. 7b, the feed rate has the most dominant effect on the surface roughness. There is a strong positive correlation between feed rate and surface roughness, which is because that the surface residual height increases with the increment of feed rate, leading to higher surface roughness. As shown in Fig. 7c, the variation of the machined surface roughness

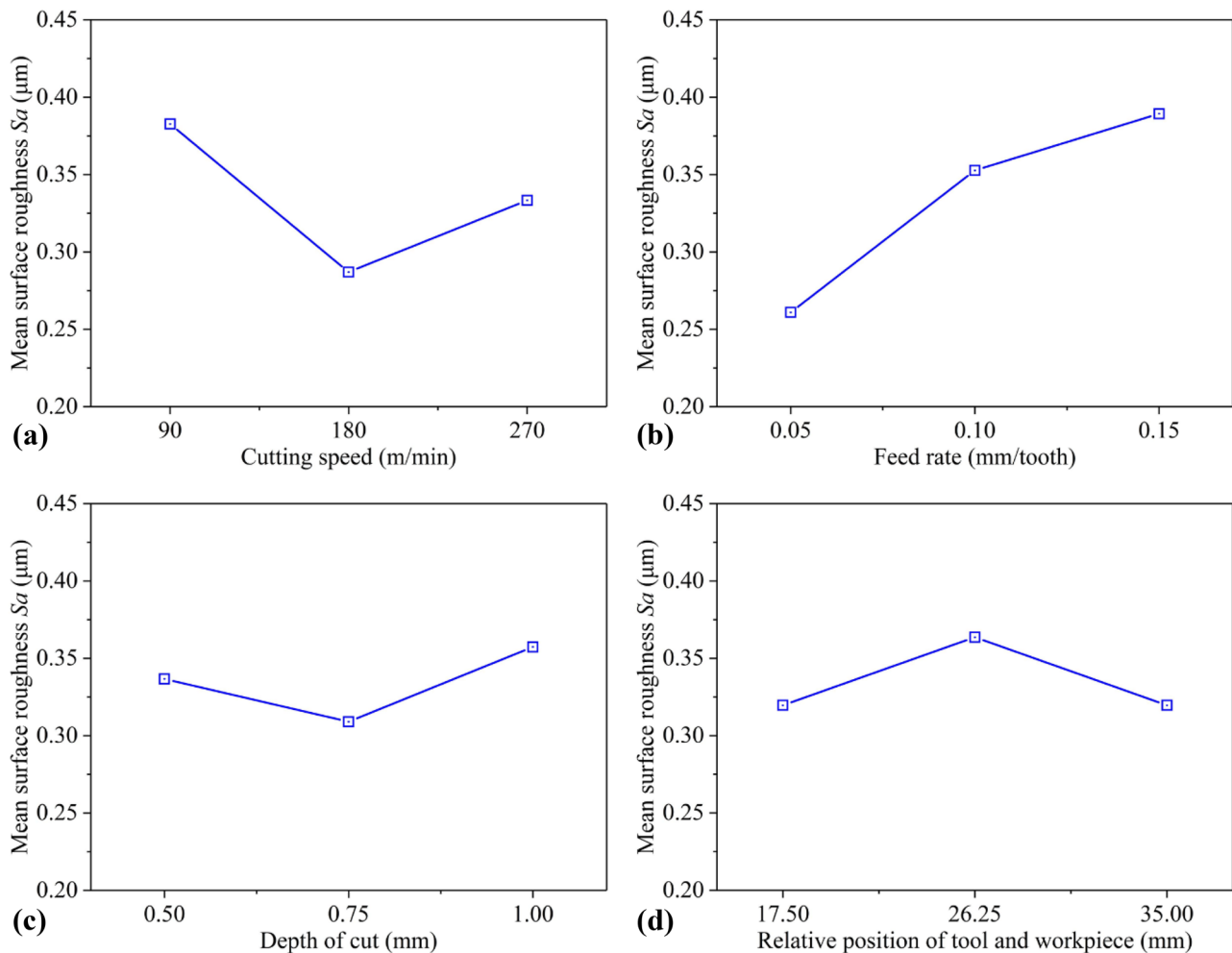


Fig. 7 Influence trends of different cutting parameters on surface roughness. **a** Cutting speed. **b** Feed rate. **c** Depth of cut. **d** Relative position of tool and workpiece

Table 7 Analysis and calculation of surface roughness

Level	v_c (m/min)	f_z (mm/tooth)	a_p (mm)	j (mm)
1	0.383	0.261	0.337	0.320
2	0.287	0.353	0.309	0.364
3	0.333	0.389	0.357	0.320
R	0.096	0.128	0.048	0.044
Rank	2	1	3	4

is relatively small with increasing of depth of cut. On the one hand, the increase in depth of cut leads to a higher cutting force. But the cutting vibration changes little due to the better rigidity of the cutting system used in this study. On the other hand, as the depth of cut increases, the cutting heat increases. However, the heat dissipation area also increases at the same time, resulting in the limited variation of cutting temperature. This does not cause excessive BUE on the cutting edge of the insert. Hence, the depth of cut has little effect on the machined surface roughness. Similar influence in surface roughness with the variation of the relative position of tool and workpiece is observed from Fig. 7d. In other words, there is no clear trend of variation between the relative position of tool and workpiece and the surface roughness, which is consistent with the conclusion drawn by Diniz et al. [15].

The influence degree of the corresponding cutting parameters on surface roughness is presented in Table 7. On the basis of various R values, the influence precedence of the four cutting parameters on surface roughness is f_z , v_c , a_p , and j for the range of tested conditions. In order to obtain the minimum surface roughness, the best combination of cutting parameters could be set to $v_c f_z a_p j$ for the range of tested conditions.

3.4 Surface residual stress

During the cutting process, the machined surface layer of the workpiece material is subjected to severe nonuniform plastic deformation due to the combined action of cutting force and cutting heat, resulting in the generation of residual stress. Extensive researches have shown that the machining induced residual stress has a crucial influence on the fatigue life and resistance to corrosion of manufacturing parts [3, 29]. As a consequence, the evaluation of residual stress at the working surface of machined components is of great significance. Thus, the residual stresses along the cutting speed direction and the feed direction were measured in this study.

As illustrated in Table 5, the residual stresses generated on the machined surface are tensile residual stresses under all cutting conditions adopted in this study. The mechanical loads can produce compressive residual stresses at the

machined surface as a result of tensile plastic deformation, while the thermal loads tend to generate tensile residual stresses. Due to low thermal conductivity (13.9 W/(m·K)) of Inconel 690, the cutting heat generated in the cutting zone cannot be transferred to the tool, chip and workpiece sub-surface region in time. Thus, a large amount of cutting heat is concentrated at the interface between tool and workpiece, which leads to the dominance of thermally induced tensile residual stresses in competition with mechanically induced compressive residual stresses at the machined surface. Furthermore, it is also found that the tensile residual stresses along the cutting speed direction are significantly greater than that along the feed direction, which is concluded that the compressive plastic deformation of the machined surface along the cutting speed direction is larger than that along the feed direction.

As shown in Fig. 8a, the tensile residual stress at the machined surface tends to be larger with an increase in cutting speed for the range of tested conditions. This is because the rise of cutting temperature at the machined surface resulting from the strengthened friction action of the tool-workpiece interface at a higher cutting speed leads to more pronounced thermal effects as comparison with the mechanical effects. As presented in Fig. 8b, with the increment of feed rate, the tensile residual stress increases significantly, which is in agreement with the conclusion of Ezilarasan et al. [8] and Hua et al. [19]. With the feed speed increasing, the more significant amount of work done to remove larger chip volume increases the heat generation in the cutting zone, and hence the thermal effects are dominant which results in more surface tensile residual stresses [30]. Also, it is observed from Fig. 8c and d that both the depth of cut and the relative position of tool and workpiece has a negligible impact on the surface residual stress. The main reason is that there is no significant change in the plastic deformation generated at the machined surface due to the small variation of the mechano-thermal loads acting on the machined surface as the depth of cut and the relative position of tool and workpiece change.

The largest R value represents that the corresponding experimental factor has the greatest impact on experimental indicators, as illustrated in Table 8. According to the calculated R value, the effect order of various cutting variables on surface residual stress along the cutting speed direction σ_{xx} is f_z , v_c , a_p , and j for the range of tested conditions. The best combination of cutting parameters corresponding to the minimum tensile residual stress along the cutting speed direction at the machined surface is $v_c f_z a_p j_3$ for the range of tested conditions. In addition, the effect order of various cutting variables on surface residual stress along the feed direction σ_{yy} is f_z , v_c , j , and a_p for the range of tested conditions. The best combination of cutting parameters

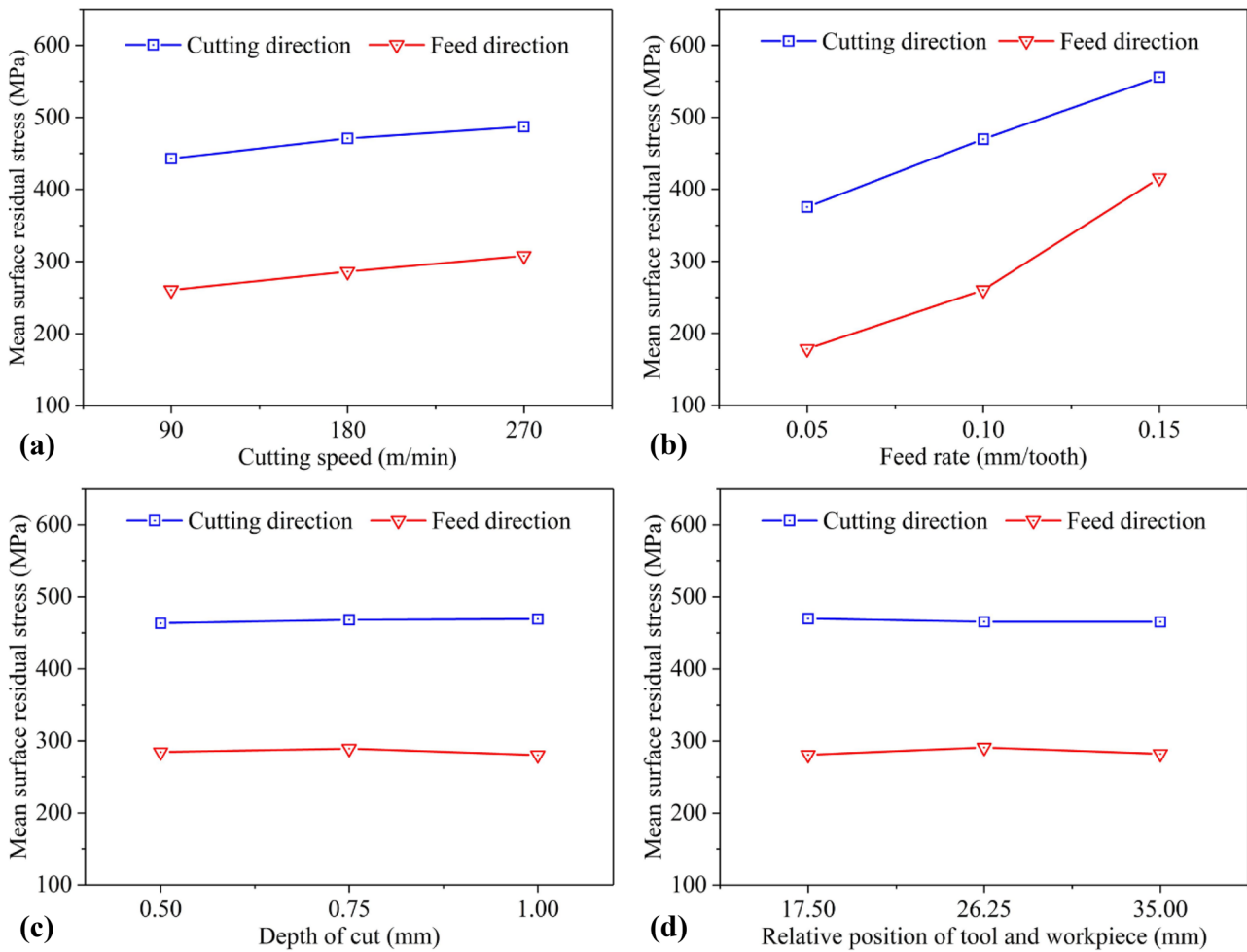


Fig. 8 Influence trends of different cutting parameters on surface residual stress. **a** Cutting speed. **b** Feed rate. **c** Depth of cut. **d** Relative position of tool and workpiece

corresponding to the minimum tensile residual stress along the feed direction at the machined surface is $v_c/f_z/a_p/j_1$ for the range of tested conditions.

3.5 Work hardening

During high-speed machining of nickel-based superalloys, the workpiece material is subjected to high cutting pressure

and temperature in the cutting zone, inducing severe work hardening generated in the machined surface layer. The DWH and depth of work hardening are often employed to quantitatively characterize the work hardening behavior of workpiece material after machining. The DWH is obtained by Eq. (3).

$$DWH = \frac{MH_s - MH_b}{MH_b} \times 100\% \tag{3}$$

Table 8 Analysis and calculation of surface residual stress

Type	Along the cutting speed direction σ_{xx} (MPa)				Along the feed direction σ_{yy} (MPa)			
	v_c (m/min)	f_z (mm/tooth)	a_p (mm)	J (mm)	v_c (m/min)	f_z (mm/tooth)	a_p (mm)	j (mm)
1	443	375	463	470	261	178	285	281
2	471	470	468	466	286	260	289	291
3	487	556	469	465	308	416	280	282
R	44	181	6	5	47	238	9	10
Rank	2	1	3	4	2	1	4	3

Table 9 DWH under all cutting conditions

Tests	No.1	No.2	No.3	No.4	No.5	No.6	No.7	No.8	No.9
DWH (%)	46.3 ± 3.4	54.2 ± 4.7	65.3 ± 4.8	53.2 ± 6.2	56.7 ± 4.3	61.1 ± 4.5	57.1 ± 5.6	63.2 ± 5.4	69.1 ± 6.2

where MH_s represents the microhardness of the machined surface, and MH_b represents the microhardness of the block material.

3.5.1 Degree of work hardening

As illustrated in Table 9, the DWH of Inconel 690 is in the range from 46.3 to 69.1% under all cutting conditions, indicating that the apparent work hardening takes place on the machined surface. For Ni-based alloy Inconel 690, $M_{23}C_6$ carbides strengthen the grain boundaries employing

precipitating as granular particles on grain boundaries [31]. This impedes the movement of dislocations, leading to the enhancement of dislocation density, thus inducing severe work hardening.

As shown in Fig. 9a, there is an increasing trend in the DWH as the cutting speed increases. For one thing, high strain rate accompanied by the increasing cutting speed exacerbates the DWH. For another, the contact time between tool and workpiece decreases with an increase in cutting speed, leading to diminished heat penetration. The similar influence trend can be found from Fig. 9b. The DWH also

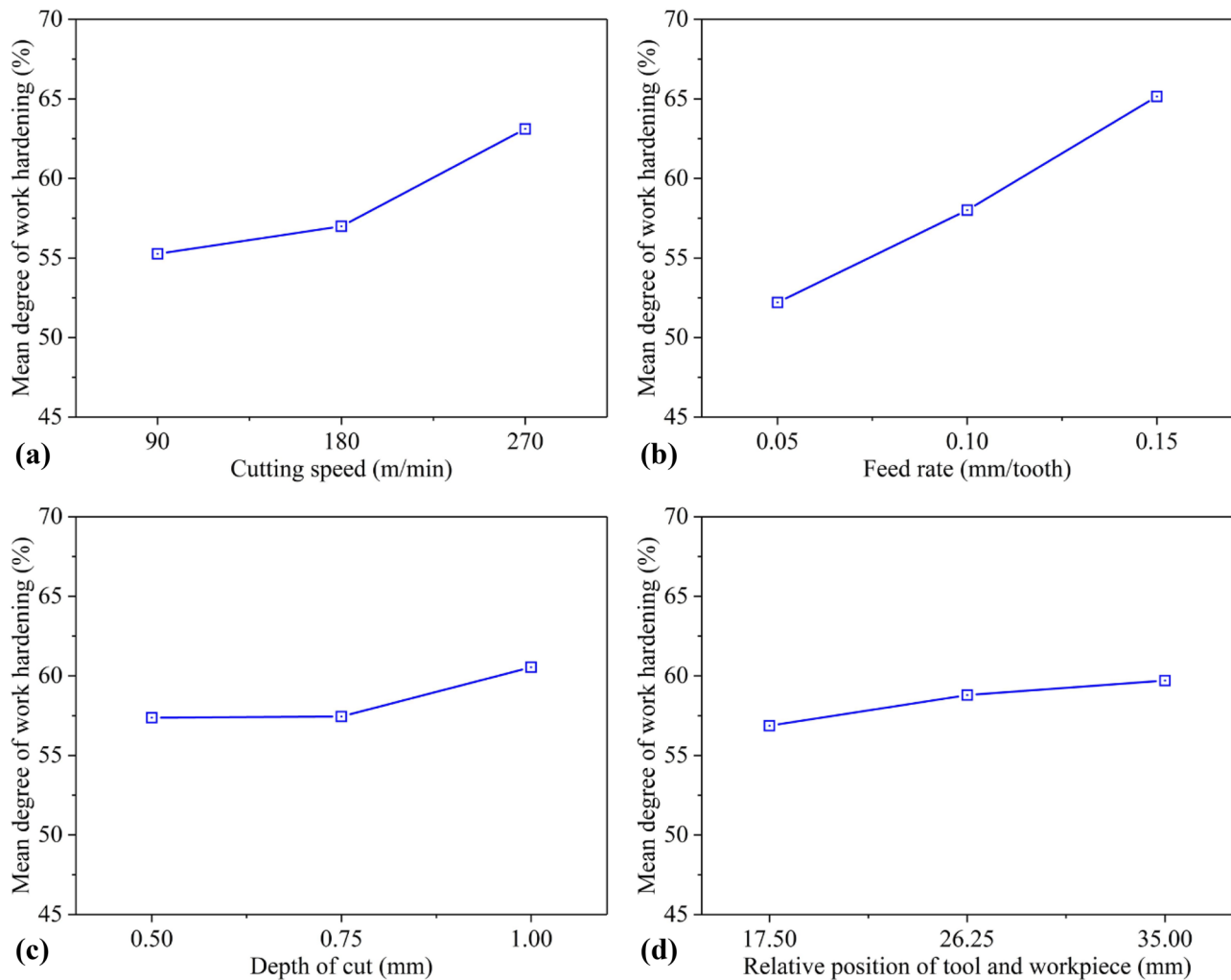


Fig. 9 Influence trends of different cutting parameters on DWH. **a** Cutting speed. **b** Feed rate. **c** Depth of cut. **d** Relative position of tool and workpiece

Table 10 Analysis and calculation of DWH

Level	v_c (m/min)	f_z (mm/tooth)	a_p (mm)	j (mm)
1	55.3	52.2	57.4	56.9
2	57.0	58.0	57.4	58.8
3	63.1	65.2	60.5	59.7
R	7.9	13.0	3.2	2.8
Rank	2	1	3	4

shows an increasing trend with the elevation of feed rate. At a higher feed rate, the greater cutting force enhances the work hardening behavior of Inconel 690 while the higher cutting temperature weakens the work hardening behavior. Under the interaction of thermo-mechanical effects, the dominance of mechanical effect makes the DWH increase as the feed rate is increased. The influence trends of the depth of cut and relative position of tool and workpiece on the DWH are presented in Fig. 9c and d, respectively. It can be observed that both the depth of cut and the relative position of tool and workpiece has no significant effects on the DWH. This may be because that the thermo-mechanical loads acting at the workpiece surface have no obvious variations with the increase of depth of cut and relative position of tool and workpiece, resulting in a small change in the degree of plastic deformation of the machined surface.

As described in Table 10, the higher the value of R is, the more significant the effect of relevant parameter on the DWH is. By comparing the R value of each cutting parameter, the effect order of cutting parameters on the DWH is f_z , v_c , a_p , and j for the range of tested conditions. In addition, the best combination of cutting parameters $v_{c1}f_{z1}a_{p1}j_1$ could be selected to obtain the minimum DWH for the range of tested conditions.

3.5.2 Depth of work hardening

The nano-hardness depth profiles of the machined surface layer under all cutting conditions were obtained by measuring the nano-hardness values at various locations below the machined surface, as shown in Fig. 10. Note that there is an obvious nano-hardness gradient in the region where the depth ranges from 3 to 30 μm beneath the machined surface. The highest nano-hardness value exists near the machined surface. Moreover, the nano-hardness value gradually drops with increasing depth until it comes close to the substrate value. Such a phenomenon may be because the effects of cutting force and cutting heat on workpiece material are rapidly declining during gradually moving away from the machined surface. Similar reduction tendency was observed by other scholars during the machining of nickel-based superalloys [32].

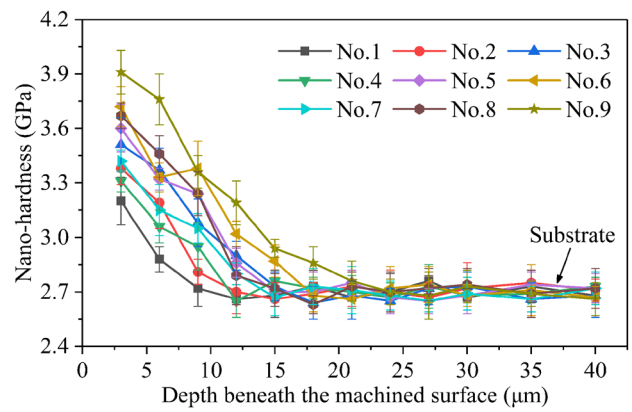


Fig. 10 Nano-hardness profiles beneath the machined surface under all cutting conditions

The depth of work hardening refers to the vertical distance from the machined surface to the non-hardened part of the as-received material. Through analyzing the corresponding nano-hardness depth profile of the machined surface layer, the depth of work hardening of each experiment was acquired as presented in Fig. 11. It is found that the depth of work hardening of machined surface layer is approximately in the range of 9–24 μm under the adopted combinations of cutting parameters. When cutting at a lower and higher cutting speed and feed rate, the depth of work hardening is about 9 μm and 24 μm , respectively.

As depicted in Fig. 12a, the cutting speed influences the depth of work hardening in a significant way. The depth of work hardening becomes greater accompanied by the elevation of cutting speed. The reason for this increasing trend is

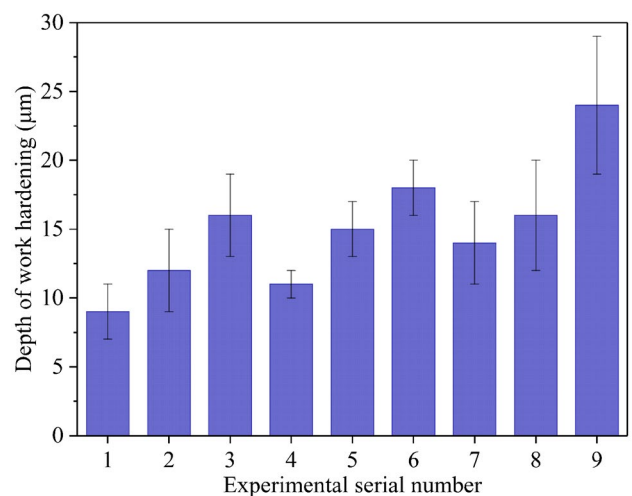


Fig. 11 Depth of work hardening of the machined surface under various cutting conditions

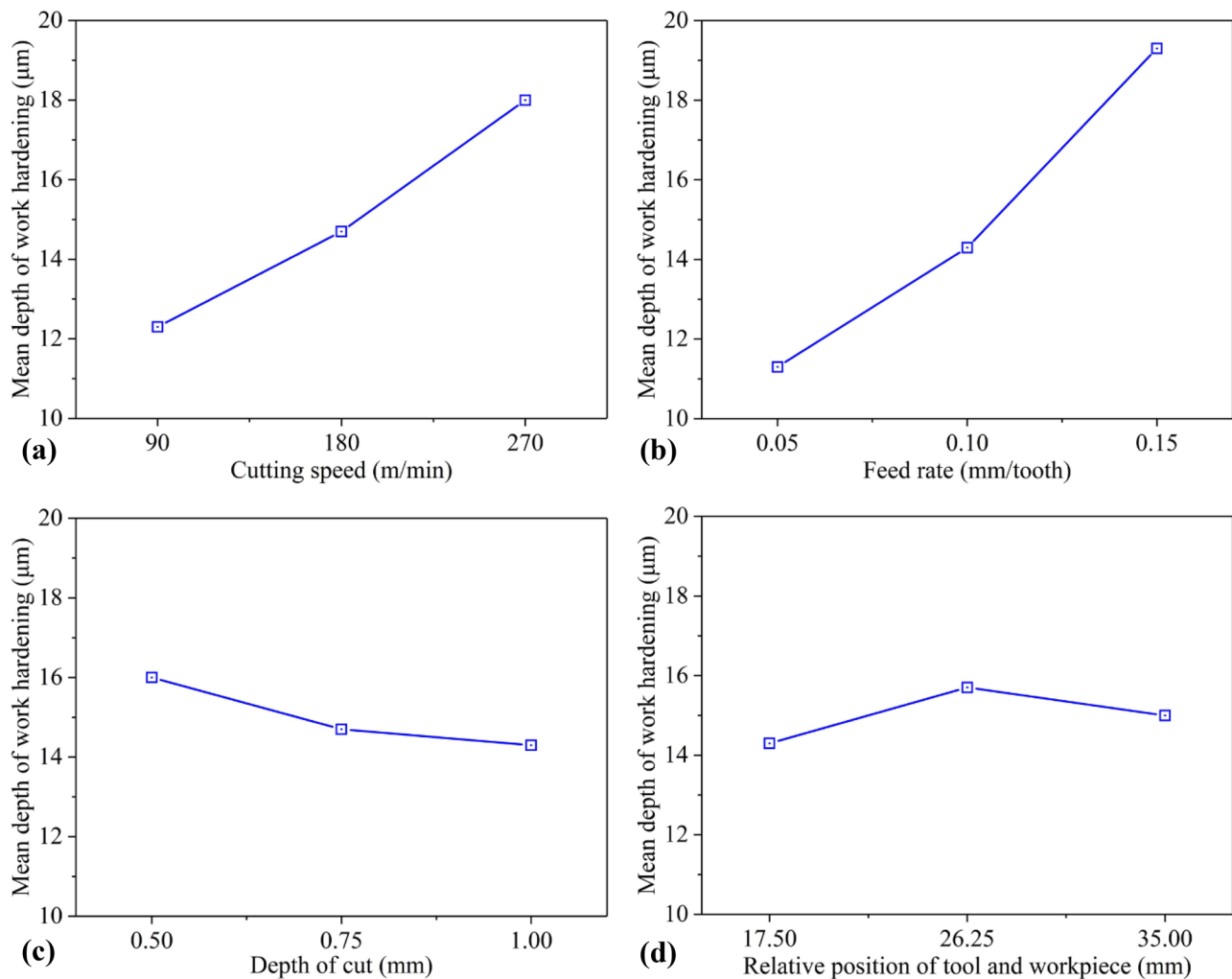


Fig. 12 Influence trends of different cutting parameters on depth of work hardening. **a** Cutting speed. **b** Feed rate. **c** Depth of cut. **d** Relative position of tool and workpiece

that the higher cutting speed makes the proportion of strain rate hardening effect over thermal softening effect become more significant. Moreover, the feed rate has the most crucial effect upon the depth of work hardening, as illustrated in Fig. 12b. As the feed rate increases, larger mechanical load results in higher plastic deformation, which induces a higher depth of work hardening [8]. In addition, it can be seen from Fig. 12c and d that the influences of depth of cut and relative position of tool and workpiece upon the depth of work hardening are little. Similarly, such phenomena may be due to no significant variation of the plastic deformation generated with the change of the depth of cut and the relative position of tool and workpiece.

According to the R value corresponding to various cutting variables in Table 11, it can be deduced that the influence precedence of various cutting parameters on the depth of work hardening is f_z , v_c , j , and a_p for the range of tested conditions. In addition, the best combination of cutting

parameters corresponding to the minimum depth of work hardening is $v_c f_z a_p j_3$ for the range of tested conditions.

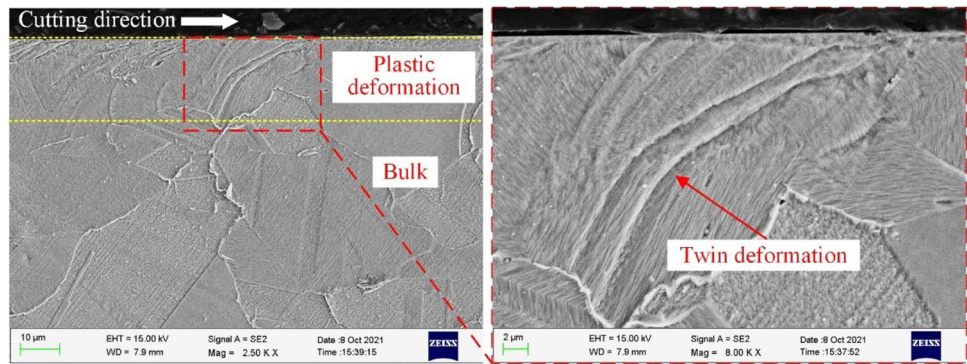
3.6 Surface microstructure

During the cutting process, severe thermo-mechanical loads acting on the tool-workpiece lead to the microstructural

Table 11 Analysis and calculation of depth of work hardening

Level	v_c (m/min)	f_z (mm/tooth)	a_p (mm)	j (mm)
1	12.3	11.3	14.3	16.0
2	14.7	14.3	15.7	14.7
3	18.0	19.3	15.0	14.3
R	5.7	8.0	1.3	1.7
Rank	2	1	4	3

Fig. 13 SEM images of machined surface microstructure under test No.9



alteration in the workpiece surface layer. This alteration can affect the functional performance of machined components in the working environment at the micro level [29, 33].

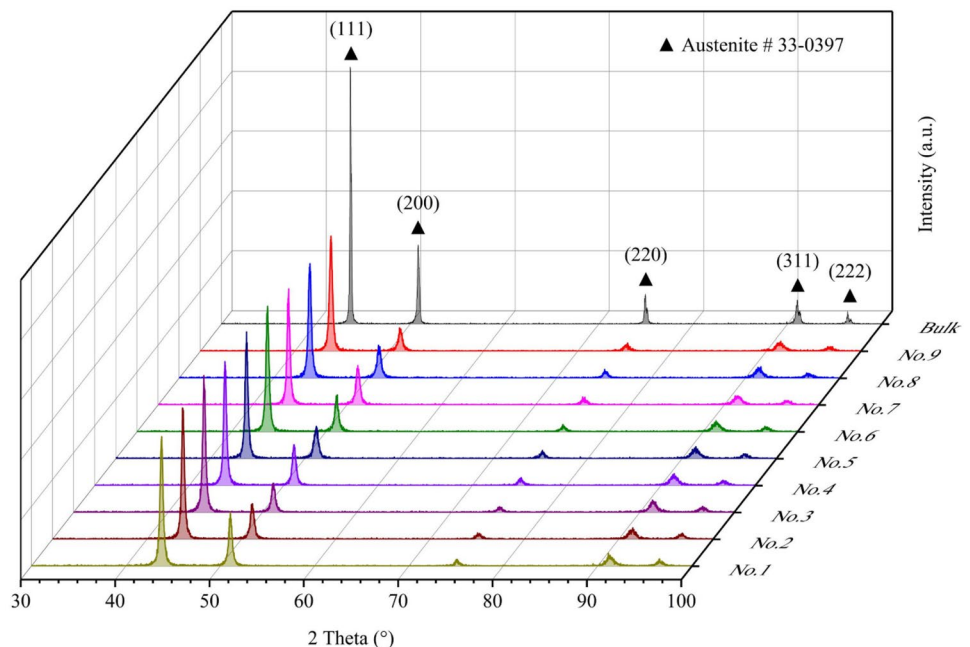
Under the cutting configuration No.9, the DWH and depth of work hardening of the machined surface are the largest for the range of tested conditions, suggesting that the surface microstructure has changed significantly under this harsh cutting condition. As shown in Fig. 13, the microstructural morphology of machined surface layer under test No.9 is observed by SEM. It is found that there are two distinct regions of plastic deformation and bulk material in the superficial layer after milling Inconel 690. In the plastic deformed zone, there is an obvious twin deformation, and the twin boundary deflects towards the cutting direction. In addition, the degree of plastic deformation in the machined surface layer decreases rapidly along the depth direction according to the deflection direction. On the contrary, the bulk material zone is not affected by the machining-induced plastic

deformation. Due to the harsh cutting condition, the workpiece surface is affected by the larger thermal and mechanical loads. The plastic deformation can reach approximately 20 μm below the machined surface, which is roughly consistent with the measured result of depth of work hardening.

3.7 X-ray diffraction analysis

The XRD patterns of the as-received material and machined surface under different cutting configurations are shown in Fig. 14. It can be seen that the peak positions of the XRD patterns for the machined surface under all cutting conditions match those observed in the as-received material. This indicates that no significant phase transformation has occurred at the machined surface under all test conditions. However, the peak broadening and significantly reduced peak intensity in the machined surface are observed compared with the as-received material. There is a sharp contrast

Fig. 14 XRD patterns of the as-received material and different machined surface



between the widened low peaks on the machined workpiece surface and the sharp high peaks on the as-received material surface. The diffraction peak broadening is usually attributed to the increase of dislocation density and grain refinement [34]. This indicates that the machined surface material undergoes severe plastic deformation after cutting, resulting in grain refinement and then broadening the diffraction peaks. Another interesting finding is that the diffraction peak intensity of the machined surface under all cutting conditions is significantly lower than that of the bulk material, which is consistent with that found by Kaynak et al. [35]. This can be explained by the existence of deformed texture at the machined surface due to severe plastic deformation.

4 Conclusion

This paper focused on investigating the cutting force and the machined surface integrity, consisting of surface morphology, surface roughness, residual stress, work hardening and microstructural alteration associated with high-speed milling of nickel-base superalloy Inconel 690 using coated cemented carbide inserts. The effects of various cutting parameters covering the cutting speed, feed rate, depth of cut and relative position of tool and workpiece on the cutting force and surface integrity were revealed. The valuable conclusions can be derived as the following.

1. The cutting force is negatively related to the cutting speed. The cutting force drops faster with the increasing of cutting speed in the lower range and drops slowly with an increase in cutting speed in the higher range. Furthermore, the cutting force displays an upward tendency with the increment of feed rate and depth of cut. However, no evident tendency between the relative position of tool and workpiece and the cutting force is presented.
2. Under various cutting conditions, the residual stress at the machined surface is tensile stress along whether the cutting speed direction or the feed direction. Such results can be attributed to the dominant thermal effects caused by the low thermal conductivity of Inconel 690 as comparison with the mechanical effects. In addition, the nano-hardness of the shallow layer for the machined surface shows the change trend of surface hardening-hardening mitigating-bulk along the depth direction.
3. Feed rate has the most significant effect upon surface integrity. With the elevation of feed rate, all of the surface roughness, tensile residual stress, DWH and depth of work hardening increase significantly. In addition, cutting speed influences the machined surface integrity in a significant way. With the increment of cutting speed, the surface roughness decreases firstly and then

increases. The increase in tensile residual stress, DWH, and depth of work hardening of the workpiece surface take place as a result of an increased cutting speed.

4. The relative position of tool and workpiece has no pronounced effect on surface integrity. The extent of such influence on residual stress and work hardening is mainly because that the mechanical load and thermal load on the workpiece surface do not change distinctly with the variation of the relative position of tool and workpiece. Similarly, the depth of cut has little influence upon surface roughness, residual stress and work hardening.
5. It is observed that there are severe plastic deformation activities such as grain deformation and twin boundary deflection in the shallow layer of machined surface. Moreover, the degree of plastic deformation in the machined surface layer decreases rapidly along the depth direction according to the twin boundary deflection direction. In addition, even under aggressive cutting condition, the machining-induced phase transformation will not occur in the machined surface material.
6. To obtain better surface integrity in face milling of Inconel 690, it is profitable to select the middle cutting speed and smaller feed rate under the permitted machining conditions. According to the research results, the relative position of tool and workpiece could be selected to achieve higher industry efficiency and lower processing costs based on the long tool life and burr minimum in industrial production. In addition, larger depth of cut could be employed to improve machining efficiency due to its ignorable effect on surface integrity.

Further experimental investigations are needed to concentrate on exploring the influence of surface integrity upon the corrosion resistance and fatigue life of the machined components made from Inconel 690, especially under various cutting speed and feed rate.

Author contribution Zhen Chen: methodology, investigation, data curation, formal analysis, visualization, writing—original draft preparation. Chuanzhen Huang: supervision, conceptualization, writing—review and editing, funding acquisition. Binghao Li: supervision, writing—reviewing and editing. Guoyan Jiang: supervision, writing—review and editing. Zhengyi Tang: writing—reviewing and editing. Jiahui Niu: writing—reviewing and editing. Hanlian Liu: supervision, writing—review and editing.

Funding This work is financially supported by Scientific Research Project for National High-level Innovative Talents of Hebei Province Full-time Introduction (2021HBQZYCY004), National Natural Science Foundation of China (52075300), Major Program of Shandong Province Natural Science Foundation (ZR2018ZA0401), Independent Training and Innovation Team Project of Jinan Science and Technology Bureau (2019GXRC009) and Leading Talents of Science and Technology Innovation in National Ten Thousand Talents Program ([2018]29).

Declarations

Conflict of interest The authors declare no competing interests.

References

- Thakur A, Gangopadhyay S (2016) State-of-the-art in surface integrity in machining of nickel-based super alloys. *Int J Mach Tools Manuf* 100:25–54. <https://doi.org/10.1016/j.ijmactools.2015.10.001>
- Choudhury IA, El-Baradie MA (1998) Machinability of nickel-base super alloys: a general review. *J Mater Process Technol* 77:278–284. [https://doi.org/10.1016/S0924-0136\(97\)00429-9](https://doi.org/10.1016/S0924-0136(97)00429-9)
- Liao ZR, la Monaca A, Murray J, Speidel A, Ushmaev D, Clare A, Axinte D, M'Saoubi R (2021) Surface integrity in metal machining - Part I: Fundamentals of surface characteristics and formation mechanisms. *Int J Mach Tools Manuf* 162:103687. <https://doi.org/10.1016/j.ijmactools.2020.103687>
- Sales WF, Schoop J, da Silva LRR, Machado AR, Jawahir IS (2020) A review of surface integrity in machining of hardened steels. *J Manuf Process* 58:136–162. <https://doi.org/10.1016/j.jmapro.2020.07.040>
- Devillez A, Le Coz G, Dominiak S, Dudzinski D (2011) Dry machining of Inconel 718, workpiece surface integrity. *J Mater Process Technol* 211:1590–1598. <https://doi.org/10.1016/j.jmatprotec.2011.04.011>
- Liu C, Ren CZ, Wang GF, Yang YW, Zhang L (2015) Study on surface defects in milling Inconel 718 super alloy. *J Mech Sci Technol* 29:1723–1730. <https://doi.org/10.1007/s12206-015-0345-1>
- Zhou JM, Bushlya V, Stahl JE (2012) An investigation of surface damage in the high speed turning of Inconel 718 with use of whisker reinforced ceramic tools. *J Mater Process Technol* 212:372–384. <https://doi.org/10.1016/j.jmatprotec.2011.09.022>
- Ezilarasan C, Kumar VSS, Velayudham A (2013) Effect of machining parameters on surface integrity in machining Nimonic C-263 super alloy using whisker-reinforced ceramic insert. *J Mater Eng Perform* 22:1619–1628. <https://doi.org/10.1007/s11665-012-0439-1>
- Thakur A, Mohanty A, Gangopadhyay S (2014) Comparative study of surface integrity aspects of Incoloy 825 during machining with uncoated and CVD multilayer coated inserts. *Appl Surf Sci* 320:829–837. <https://doi.org/10.1016/j.apsusc.2014.09.129>
- Soo SL, Hood R, Aspinwall DK, Voice WE, Sage C (2011) Machinability and surface integrity of RR1000 nickel based superalloy. *CIRP Ann-Manuf Technol* 60:89–92. <https://doi.org/10.1016/j.cirp.2011.03.094>
- Thakur A, Gangopadhyay S, Mohanty A (2015) Investigation on some machinability aspects of Inconel 825 during dry turning. *Mater Manuf Process* 30:1026–1034. <https://doi.org/10.1080/10426914.2014.984216>
- Liang XL, Liu ZQ, Wang B (2019) State-of-the-art of surface integrity induced by tool wear effects in machining process of titanium and nickel alloys: a review. *Measurement* 132:150–181. <https://doi.org/10.1016/j.measurement.2018.09.045>
- Umbrello D (2013) Investigation of surface integrity in dry machining of Inconel 718. *Int J Adv Manuf Technol* 69:2183–2190. <https://doi.org/10.1007/s00170-013-5198-0>
- Li Q, Gong YD, Cai M, Liu MJ (2017) Research on surface integrity in milling Inconel718 superalloy. *Int J Adv Manuf Technol* 92:1449–1463. <https://doi.org/10.1007/s00170-017-0080-0>
- Diniz AE, Caldeirani J (1999) Influence of the relative positions of tool and workpiece on tool life, tool wear and surface finish in the face milling process. *Wear* 232:67–75. [https://doi.org/10.1016/S0043-1648\(99\)00159-3](https://doi.org/10.1016/S0043-1648(99)00159-3)
- Imran M, Mativenga PT, Gholinia A, Withers PJ (2014) Comparison of tool wear mechanisms and surface integrity for dry and wet micro-drilling of nickel-base superalloys. *Int J Mach Tools Manuf* 76:49–60. <https://doi.org/10.1016/j.ijmactools.2013.10.002>
- Jiang HW, Wang CY, Ren ZW, Yi YL, He L, Zhao XF (2021) Influence of cutting velocity on gradient microstructure of machined surface during turning of high-strength alloy steel. *Mater Sci Eng A* 819:141354. <https://doi.org/10.1016/j.msea.2021.141354>
- Cai XJ, Qin S, Li JL, An QL, Chen M (2014) Experimental investigation on surface integrity of end milling nickel-based alloy-Inconel 718. *Mach Sci Technol* 18:31–46. <https://doi.org/10.1080/10910344.2014.863627>
- Hua Y, Liu ZQ (2018) Experimental investigation of principal residual stress and fatigue performance for turned nickel-based superalloy Inconel 718. *Materials* 11:879. <https://doi.org/10.3390/ma11060879>
- Hua Y, Liu ZQ (2018) Effects of cutting parameters and tool nose radius on surface roughness and work hardening during dry turning Inconel 718. *Int J Adv Manuf Technol* 96:2421–2430. <https://doi.org/10.1007/s00170-018-1721-7>
- Pawade RS, Joshi SS, Brahmankar PK (2008) Effect of machining parameters and cutting edge geometry on surface integrity of high-speed turned Inconel 718. *Int J Mach Tools Manuf* 48:15–28. <https://doi.org/10.1016/j.ijmactools.2007.08.004>
- Guo SL, Li DF, Pen HJ, Guo QM, Hu J (2011) Hot deformation and processing maps of Inconel 690 superalloy. *J Nucl Mater* 410:52–58. <https://doi.org/10.1016/j.jnucmat.2010.12.309>
- Lee WS, Liu CY, Sun TN (2005) Dynamic impact response and microstructural evolution of Inconel 690 superalloy at elevated temperatures. *Int J Impact Eng* 32:210–223. <https://doi.org/10.1016/j.ijimpeng.2004.09.007>
- Sen B, Gupta MK, Mia M, Mandal UK, Mondal SP (2020) Wear behaviour of TiAlN coated solid carbide end-mill under alumina enriched minimum quantity palm oil-based lubricating condition. *Tribol Int* 148:106310. <https://doi.org/10.1016/j.triboint.2020.106310>
- Sen B, Mia M, Mandal UK, Mondal SP (2020) Synergistic effect of silica and pure palm oil on the machining performances of Inconel 690: a study for promoting minimum quantity nano doped-green lubricants. *J Clean Prod* 258:120755. <https://doi.org/10.1016/j.jclepro.2020.120755>
- Makhesana MA, Patel KM, Khanna N (2022) Analysis of vegetable oil-based nano-lubricant technique for improving machinability of Inconel 690. *J Manuf Process* 77:708–721. <https://doi.org/10.1016/j.jmapro.2022.03.060>
- Jiang FL, Liu ZQ, Wan Y, Shi ZY (2013) Analytical modeling and experimental investigation of tool and workpiece temperatures for interrupted cutting 1045 steel by inverse heat conduction method. *J Mater Process Technol* 213:887–894. <https://doi.org/10.1016/j.jmatprotec.2013.01.004>
- Liang XL, Liu ZQ, Yao GH, Wang B, Ren XP (2019) Investigation of surface topography and its deterioration resulting from tool wear evolution when dry turning of titanium alloy Ti-6Al-4V. *Tribol Int* 135:130–142. <https://doi.org/10.1016/j.triboint.2019.02.049>
- Liu GL, Huang CZ, Zhao B, Wang W, Sun SF (2021) Effect of machined surface integrity on fatigue performance of metal workpiece: a review. *Chin J Mech Eng* 34:118. <https://doi.org/10.1186/s10033-021-00631-x>
- Sharman ARC, Hughes JI, Ridgway K (2015) The effect of tool nose radius on surface integrity and residual stresses when turning Inconel 718 (TM). *J Mater Process Technol* 216:123–132. <https://doi.org/10.1016/j.jmatprotec.2014.09.002>
- Zhao X, Wang M, Hao XC, Zha XD, Gao M, Ma YC, Liu K (2021) Precipitation of dendritic M23C6 carbides in alloy 690 during continuous cooling. *J Alloy Compd* 851:156694. <https://doi.org/10.1016/j.jallcom.2020.156694>

32. Liang XL, Liu ZQ, Ren XP, Wang B (2021) Tool wear induced the gradient distribution of surface integrity with process-micro-structure-property characteristics after turning Ti-6Al-4 V. *J Manuf Process* 70:570–577. <https://doi.org/10.1016/j.jmapro.2021.09.007>
33. Wojciechowski S, Matuszak M, Powalka B, Madajewski M, Maruda RW, Krolczyk GM (2019) Prediction of cutting forces during micro end milling considering chip thickness accumulation. *Int J Mach Tools Manuf* 147:103466. <https://doi.org/10.1016/j.ijmachtools.2019.103466>
34. Nie XF, He WF, Zhou LC, Li QP, Wang XD (2014) Experiment investigation of laser shock peening on TC6 titanium alloy to improve high cycle fatigue performance. *Mater Sci Eng A* 594:161–167. <https://doi.org/10.1016/j.msea.2013.11.073>
35. Kaynak Y, Gharibi A, Yilmaz U, Koklu U, Aslantas K (2018) A comparison of flood cooling, minimum quantity lubrication and high pressure coolant on machining and surface integrity of titanium Ti-5553 alloy. *J Manuf Process* 34:503–512. <https://doi.org/10.1016/j.jmapro.2018.06.003>

Publisher's Note Springer Nature remains neutral with regard to jurisdictional claims in published maps and institutional affiliations.